RSC Advances

PAPER

View Article Online
View Journal | View Issue

Cite this: *RSC Adv.*, 2020, **10**, 3826

Interfacial effect of dual ultra-thin SiO_2 core–triple shell Au@SiO_2@Ag@SiO_2 for ultra-sensitive trinitrotoluene (TNT) detection†

Bingxin Lu,[a] Qi Qi,[a] Yang Wang,[b] Huaiqiu Chang,[c] Jin Zhai *[a] and Tingting You*[a]

Received 30th August 2019
Accepted 2nd November 2019

DOI: 10.1039/c9ra06902j

rsc.li/rsc-advances

Nanostructured hybrid Au@SiO_2@Ag@SiO_2 was developed, which greatly enhanced the surface plasmon resonance effect due to the interfacial effect of dual ultra-thin SiO_2 in which the double-superimposed long-range plasmon transfer between Au and Ag and determinand molecules. In addition, the interfacial effect between the inner and outermost silica layer can contribute to the presence of an amplified electric field between Au core and Ag shell, which prevents aggregation and oxidation of nanoparticles. At the same time, the influence of the amount of silica in SiO_2 shells on the Surface Enhanced Raman Scattering (SERS) was explored by controlling the experimental conditions. In our experiments, the ultrathin silica coating Au@SiO_2@Ag@SiO_2 showed the best SERS performance, generating an analytical enhancement factor (AEF) of 5×10^6. At the same time, nanoparticles modified by 4-aminothiophenol (4-ATP) can detect 2,4,6-TNT as low as 2.27×10^{-6} ppb (10^{-14} M) and exhibit excellent versatility in the detection of nitroaromatics. The results demonstrated that the interfacial effect of double-layer dielectric silica achieved the localized surface plasmon resonance enhancement effect in Au@SiO_2@Ag@SiO_2.

Introduction

Precious metals at the nanometer scale have special optoelectronic properties; Au and Ag nanoparticles have attracted wide interest due to the localized surface plasmon resonance (LSPR) effect.[1–4] However, the LSPR performance of metal nanoparticles is reduced because of oxidation and aggregation during application.[5,6] Therefore, a variety of core–shell structure materials have been developed to suppress the adverse reactions occurring at the interface during the contact of the nanoparticles with the working atmosphere.[7–10] In addition, various shell materials can be used for different applications, in order to achieve the above effects and improve the performance of the materials, for example, Fe_3O_4@Ag/SiO_2/Au,[11] Ag@SiO_2,[12] Au@SiO_2,[13] Ag@TiO_2 (ref. 14) and *et al.* In terms of Au and Ag precious metals, the hybrid structure of Au and Ag has stronger surface plasmon resonance effect than that of single component nanoparticles, which makes nanomaterials with two or more component hybrid structures widely used in surface-enhanced Raman scattering and plasma sensing.[15,16] The use of plasmonic nanoparticles which were coated with SiO_2 shells for Raman detection is referred as shell-isolated nanoparticle-enhanced Raman spectroscopy (SHINERS).[13] The shell-isolated nanoparticles used in shell-isolated mode can solve the following disadvantages: (1) the adsorbed impurity molecules may generate a stronger signal than the probe molecules. (2) Direct contact may cause charge transfer between the plasmonic nanoparticles and the metal substrate to cause signal distortion. (3) The direct adsorption on the metal surface may change the electron density of adsorbed molecules, which may subsequently change the adsorption behavior of the molecules.[17,18] The interfacial effect between the inner and outermost silica layer can contribute to the present of an amplified electric field between Au core and Ag shell and prevent the aggregation and oxidation of the nanoparticles, so the passivation layer can enhance the surface plasmon resonance effect.[19]

In this work, we studied the interfacial effect of double-layer dielectric silica that can enhance the surface plasmon resonance effect in Au@SiO_2@Ag@SiO_2. Preparation procedure of Au@SiO_2@Ag@SiO_2 and mechanism of TNT detection with this substrate were shown in Scheme 1. Dual SiO_2 layers were dispersed on the interface of Au and Ag. The plasmon undergoes long-range transfer between Au and Ag as the SiO_2 insertion, which can enhance surface plasmon resonance effect.[20] We used the 3D-FDTD solution (http://www.lumerical.com) to calculate optical spectra and electromagnetic field enhancement around nanostructure by numerically solving Maxwell's differential equations[21–23] with the purpose of demonstrating the occurrence of plasmon long-range transfer. The outermost layer SiO_2 layer can prevent aggregation and oxidation of nanoparticles and

[a]*Key Laboratory of Bio-Inspired Smart Interfacial Science and Technology of Ministry of Education, School of Chemistry, Beihang University, China. E-mail: zhaijin@buaa.edu.cn*

[b]*Institute of Chemistry Chinese Academy of Sciences, China*

[c]*National Center for Nanoscience and Technology, China*

† Electronic supplementary information (ESI) available. See DOI: 10.1039/c9ra06902j

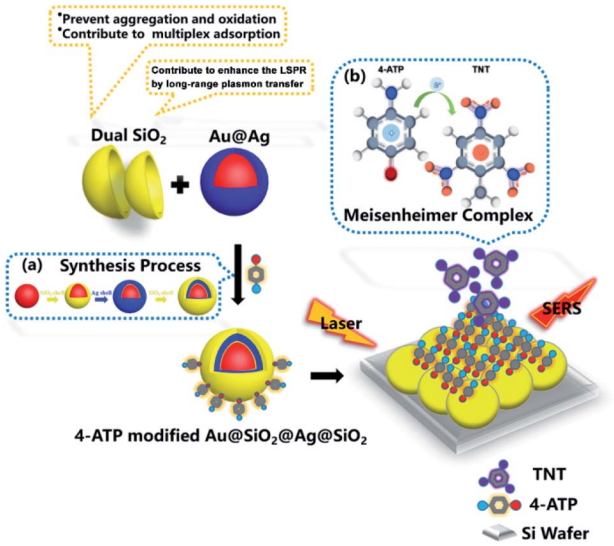

Scheme 1 $Au@SiO_2@Ag@SiO_2$ modified with 4-ATP of SERS detection protocol for TNT, (a) synthesis process of $Au@SiO_2@Ag@SiO_2$ and (b) donor–acceptor (D–A) interaction between TNT and 4-ATP of Meisenheimer complex.

benefit the interfacial effect of plasmon transfer to enhance the surface plasmon resonance effect of the material. The Raman scattering of molecules was enhanced because of the dual silica layer existing in the $Au@SiO_2@Ag@SiO_2$. TNT was identified by using a Meisenheimer complex consisting of TNT and 4-ATP, which was adsorbed onto the nanoparticles by the formation of hydrogen bonds.[24] $Au@SiO_2@Ag@SiO_2$ and other four nanoparticles ($Au@Ag@SiO_2$, Au@Ag, $Ag@SiO_2$, and $Au@SiO_2@Ag$) were used as substrate material for SERS detection of TNT to demonstrate that the $Au@SiO_2@Ag@SiO_2$ exhibited an optimal enhanced LSPR effect. The result displays that the $Au@SiO_2@Ag@SiO_2$ has the best SERS performance, yield an AEF of 5×10^6. Meanwhile, the nanoparticles modified with 4-ATP can detect 2,4,6-TNT as low as 2.27×10^{-6} ppb (10^{-14} M) and show excellent versatility in detecting nitroaromatic compounds. The result demonstrated that the double-layer dielectric silica in the nanostructure would enhance the LSPR effect because of the interfacial effect. This nanomaterial presents potential applications for future developments in photoelectricity and SERS detection.

Experimental

Materials

Chloroauric acid (AR), sodium citrate, (3-aminopropyl) triethoxysilane (APTES, 97%), sodium silicate (AR), ascorbic acid (AR), silver nitrate (AR) and sodium hydroxide (AR) were purchased from Sinopharm Corporation. Rhodamine 6G (R6G, 99%) and 4-aminothiophenol (99%) were purchased from Sigma.

Synthesis of Au nanoparticles

1.4 mL of sodium citrate (1%) was added to 200 mL of a boiling aqueous solution containing chloroauric acid (0.01%). The solution was boiled for 15 min and then cooled to room temperature.

Synthesis of $Au@SiO_2$ nanoparticles

1 mM APTES was added to the 30 mL Au NPs solution under vigorous magnetic stirring in 15 min. Then volume of a 0.54 wt% sodium silicate solution (3.0, 3.1, 3.2, 3.3 mL) was added to the solution, again under vigorous magnetic stirring under 100 °C. The $Au@SiO_2$ core–shell nanomaterials were obtained.

Synthesis of $Au@SiO_2@Ag@SiO_2$ nanoparticles

540 μL 100 mM of L-ascorbic acid, 135 μL 100 mM of $AgNO_3$, and 675 μL 100 mM of NaOH were added to a beaker containing 30 mL of as-prepared $Au@SiO_2$ NPs at room temperature. Then, 1 mM (3-aminopropyl) triethoxysilane (APS) was added to the $Au@SiO_2@Ag$ solution under vigorous magnetic stirring in 15 min. Then volume of a 0.54 wt% sodium silicate solution (3.0, 3.1, 3.2, 3.3 mL) was added to the solution, again under vigorous magnetic stirring under 100 °C. The resulting particles were centrifuged at 8000 rpm for 5 min. The $Au@SiO_2@Ag@SiO_2$ core–triple shells nanomaterials were obtained.

TNT and R6G detection

Relevant nanoparticles $Ag@SiO_2$, $Au@Ag@SiO_2$, Au@Ag, and $Au@SiO_2@Ag$ were synthesized with similar size and used as substrate for SERS measurement. These nanoparticles were respectively incubated in 10^{-6} M R6G aqueous solutions for 30 min. And the unbound R6G molecules were removed by centrifugation, then, 5 μL samples were pipetted onto the silicon wafer, drying at room temperature. The Raman spectra were measured at 633 nm excitation and laser power of 1.5 mW with acquisition time of 3 s. For calculating analytical enhancement factor, Raman spectra 0.1 M R6G solution was tested under non-SERS substrate conditions. Pre-prepared $Au@SiO_2@Ag@SiO_2$ NPs was immersed into the 4-ATP of varied concentration from 10^{-16} M to 10^{-10} M for 4 h to evaluate SERS properties of it. At last, $Au@SiO_2@Ag@SiO_2$ modified with 4-ATP was formed by immersing $Au@SiO_2@Ag@SiO_2$ into 10^{-8} M 4-ATP to detect TNT, dinitrotoluene (DNT) and nitrobenzene (NB). We dispersed 2,4,6-TNT of 10^{-14} M to 10^{-11} M (ethanol was used as solvent) on 4-ATP-modified $Au@SiO_2@Ag@SiO_2$. Furthermore, 10^{-12} M analyte 2,4,5-TNT, 2,3,6-TNT, 2,3,4-TNT, 2,3-DNT and NB were detected to reveal the universal application of this nanoparticle. Each step above was followed by the washing procedure to remove the unbound molecules. All Raman spectra were collected using Jobin Yvon (Laboratory RAM HR800) confocal micro-Raman spectrometer equipped with multichannel charge coupled detector. The Raman spectra were obtained by 633 nm photoexcitation and measured at laser power of 1.5 mW with acquisition time of 10 s.

Results and discussion

Morphology and structure

Fig. 1a–c showed the transmission electron microscope images of the core–shell structured Au@SiO_2@Ag@SiO_2. As reported previously, an electron density image of Au core is darker than that of the Ag shell because of the difference in electron density of Au and Ag atoms, which provides sufficient contrast to distinguish the Au core from the Ag shell.[25] To further demonstrate the core–triple shell structure, we chose the elemental mapping from high angle annular dark field scanning transmission electron microscopy (HAADF-STEM) imaging to reveal the Au@SiO_2@Ag@SiO_2 core–triple shell structure. The STEM image of Au@SiO_2@Ag@SiO_2 was shown in Fig. 1d. In addition, the mapping images of Au core (green), Ag shell (yellow), oxygen (red) and dual SiO_2 shells (orange) were observed respectively (Fig. 1e–h), which proved the core–triple shell structure of Au@SiO_2@Ag@SiO_2.

Effect of dual SiO_2

Then studies on interfacial effect of dual SiO_2 have focused on comparison of similar structural nanoparticles of single SiO_2 and none. We fabricated relevant nanospheres Ag@SiO_2, Au@Ag@SiO_2, Au@Ag and Au@SiO_2@Ag. These obtained nanoparticles possessed a uniform and well-defined core–shell structure. The scanning electron microscopy (SEM) of assembled nanoparticles confirms the actual structure and size in Fig. S1.† The UV-vis-NIR spectra of the Au@SiO_2@Ag@SiO_2, Au@Ag@SiO_2, Au@Ag, Ag@SiO_2, and Au@SiO_2@Ag NPs were shown in Fig. S2.† It could be seen that Au@SiO_2@Ag@SiO_2 NPs presented different absorption intensities between 350 nm and 800 nm, which certificated that the LSPR effect remained existing under the excitation wavelength between 350 nm and 800 nm.

R6G, a common molecule probe for testing SERS activity, was used to reveal the SERS enhancement. The fluorescence interference might happen if we chose the excitation wavelength corresponding to SPR max. Considering the fluorescence excitation maximum of R6G is 527 nm,[26] we chose the excitation wavelength of 633 nm, in which the Surface Plasmon Resonance (SPR) existed, as the excitation wavelength of Raman to avoid the fluorescence interference.[27] The characteristic absorption bands of R6G in the range from 800 cm^{-1} to 2000 cm^{-1} were shown in Fig. 2a. For the clarity of comparison, the SERS intensities of characteristic peaks of R6G at 1186, 1316, 1514 and 1653 cm^{-1} were showed in Fig. 2b.[28] The characteristic peaks of 1186 cm^{-1} and 1316 cm^{-1} were assigned to the C–H in-plane bending vibration and the N–H in-plane bending vibration, respectively. And the characteristic peaks of 1514 cm^{-1} and 1653 cm^{-1} were attributed to the C–C stretching vibration. Fig. 2b showed the intensity of R6G with Au@SiO_2@Ag@SiO_2, Au@Ag@SiO_2, Au@Ag, Ag@SiO_2, and Au@SiO_2@Ag NPs. Among these particles, Au@SiO_2@Ag@SiO_2 improved the highest signal enhancement.

Obviously, introducing SiO_2 layer into bimetallic nanospheres resulted in a remarkable increase of SERS intensity. The SERS effect of Au@SiO_2@Ag@SiO_2 at the same concentration of R6G was superior to other nanoparticles, demonstrating that the interfacial effect of dual SiO_2 layer would improve the SERS effect of substrate material. Raman spectra of Au@SiO_2@Ag@SiO_2 and Au@Ag@SiO_2 indicated that the interfacial effect of the inner SiO_2 would enhance the surface plasmon resonance effect of nanoparticles. Meanwhile, it is found that Au@Ag@SiO_2 presented higher SERS intensity than Au@Ag and Au@SiO_2@Ag, demonstrating that outer interfacial SiO_2 can avoid oxidation and aggregation of unmodified metallic nanoparticles of Au and Ag[29] and benefit the plasmon transfer between molecules and nanoparticles. Moreover, the outer ultrathin SiO_2 layer can avoid change of electron density of adsorbed molecules, which may subsequently change the adsorption behavior of the molecules.[17,18] Thus, the interfacial effect of outermost layer can enhance the surface plasmon resonance effect. Compared to Ag@SiO_2, the SERS signal of Au@Ag is stronger, which evidenced bimetallic Au@Ag improved SERS activity. Considering the silver was easy to be oxidized, agglomeration occurred in Au@SiO_2@Ag, which weakened SERS enhancement. Therefore, the aggregation of particles did not occur with interfacial silica coating. Superior SERS performance of Au@SiO_2@Ag@SiO_2 was clearly observed due to the dual SiO_2 layers.

Moreover, this Au@SiO_2@Ag@SiO_2 materials yielded a large SERS enhancement of 10^6–10^7 in R6G solution. To calculate the enhancement effect, we employed the value of AEF, which is

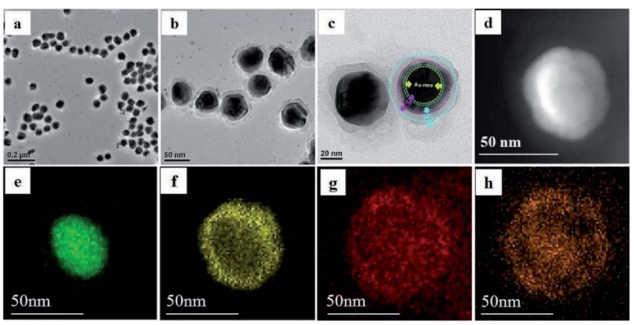

Fig. 1 (a–c) TEM of Au@SiO_2@Ag@SiO_2 NPs. (d–h) The HAADF-STEM image of Au@SiO_2@Ag@SiO_2 NPs (d) and mapping of Au core: green (e); Ag shell: yellow (f); oxygen: red (g) and dual SiO_2 shell: orange (h).

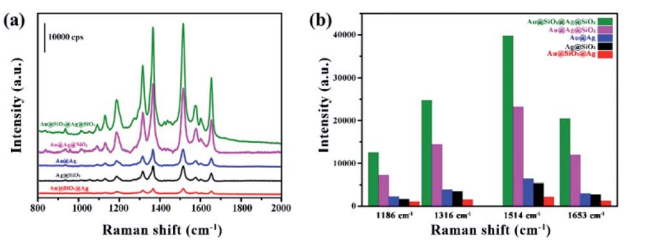

Fig. 2 (a) Comparison of SERS spectra and (b) intensity of R6G with Au@SiO_2@Ag@SiO_2, Au@Ag@SiO_2, Au@Ag, Ag@SiO_2, and Au@SiO_2@Ag NPs. All Raman spectra were measured at laser power of 1.5 mW with acquisition time of 3 s. Intensities were displayed respectively at 1186, 1316, 1514, 1653 cm^{-1}.

defined as $(C_{SERS}/C_{RS})/(I_{RS}/I_{SERS})$.[30] We considered the R6G solution with concentration C_{RS} (10^{-1} M), which produced a Raman signal I_{RS} under non-SERS conditions as shown in Fig. S4.† Under identical experimental conditions (laser wavelength, laser power, microscope objective or lenses, spectrometer, *etc.*) the SERS signal intensity (I_{SERS}) was obtained by Raman detection of 10^{-6} M (C_{SERS}) of the R6G on the $Au@SiO_2@Ag@SiO_2$ substrate. From this definition, we calculated the value of AEF was 5×10^6.

Control of the amount of interfacial SiO_2

It was known that interfacial SiO_2 shell could prevent the changes of electron density of adsorbed molecules, and the amount of SiO_2 played a critical role in SERS.[13] Herein, we encapsulated Au and Au@Ag NPs with different the amount of SiO_2 by adjusting the volume of sodium silicate (3.0, 3.1, 3.2, 3.3 mL) during the experiment. When the amount of double SiO_2 in Au @ SiO_2 @Ag @ SiO_2 was controlled, the volume of sodium silicate used in the two processes remained the same. The transmission electron microscopy (TEM) images of $Au@SiO_2@Ag@SiO_2$ with different amounts of sodium silicate were shown in Fig. S3.† The R6G was used to evaluate the SERS properties of the $Au@SiO_2@Ag@SiO_2$ nanoparticles with different thickness of silica. Compared with $Au@SiO_2$, the dual-layer SiO_2 contributed to stronger SERS signal as shown in Fig. 3. The Raman spectra intensity of R6G on $Au@SiO_2@Ag@SiO_2$ (Fig. 3b) exhibited 6 times higher than that on $Au@SiO_2$ (Fig. 3a) with the same thickness of the silica layers. The inserts of Fig. 3 showed that the intensity at 1514 cm^{-1} with different volume of sodium silicate. With the growth of the amount of SiO_2 in nanoparticles, the SERS effect initially increased and then decreased. Experimental results showed that the SERS effect of the nanoparticles is optimal when the amount of sodium silicate is 3.2 mL. Under this condition, the SERS intensity of $Au@SiO_2@Ag@SiO_2$ was about double and five-fold greater than the amount of sodium silicate of 3.3 mL and 3.0 mL, respectively. These can be ascribed to that undesirable thickness of SiO_2 layer limits the SERS effect as surface plasmon damping and dynamic depolarization.[31,32] And dual interfacial SiO_2 layers between the two metals were beneficial to bring an enhancement of SERS signal.

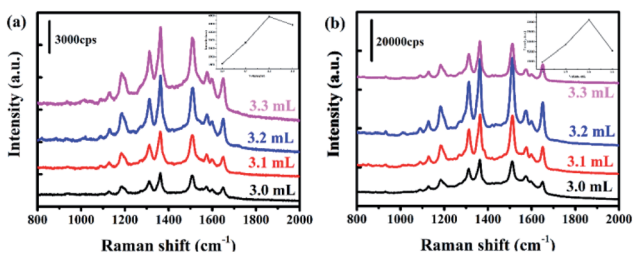

Fig. 3 SERS spectra of R6G with (a) $Au@SiO_2$ and (b) $Au@SiO_2@Ag@SiO_2$ with gradient SiO_2 thickness by control the volume of sodium silicate (3.0, 3.1, 3.2, 3.3 mL). For $Au@SiO_2@Ag@SiO_2$, the thickness of inner and outer SiO_2 layer are same there. The inserts of figure showed that the intensity at 1514 cm^{-1} with different volume of sodium silicate.

3D-FDTD simulations

The 3D-FDTD solution (http://www.lumerical.com) was introduced to calculate optical spectra and electromagnetic field enhancement around nanostructure by numerically solving Maxwell's differential equations.[21–23] $Au@SiO_2@Ag@SiO_2$ model and $Ag@SiO_2$ model with similar size were constructed to explain the long-range plasmon transfer effect. Au core was built as a sphere object with a radius of 25 nm. The thickness of SiO_2 shell, Ag shell and SiO_2 shell was 5, 15 and 5 nm, respectively. Incident light source was propagated from the z axis and polarized along x direction. The wavelength was set to be 633 nm in all simulations. Data of dielectric constants were from Johnson and Christy. The Yee cell size in FDTD simulation was considered to meet the accuracy needed by both wavelength and object parameters and to avoid too large memory resources and computation time required. Fig. S5† showed the 2D patterns of E-field amplitude ($|E|$) of $Ag@SiO_2$ model (a and b) and $Au@SiO_2@Ag@SiO_2$ model (c and d) of similar particle size. As shown in Fig. S5,† the maximum E-field amplitude ($|E|$) for $Au@SiO_2@Ag@SiO_2$ model and $Ag@SiO_2$ model was 4.6 and 3.4, respectively, which demonstrated that the electric field enhancement of $Au@SiO_2@Ag@SiO_2$ increased compared with $Ag@SiO_2$ of similar particle size. In addition, the maximum enhancement was mainly in gap region between Au core and Ag layer as shown in Fig. S5(c and d).† This enhancement was transferred to the surface of the nanoparticles through the outer layer of silica, achieving the enhancement of LSPR, which were considered to originate from the long-range plasmon transfer between Au and Ag.

Sensitivity of TNT detection

$Au@SiO_2@Ag@SiO_2$ NPs has been shown to be an excellent material for SERS. Subsequently, 4-ATP as the unique Raman signature could capture TNT molecule by formation of the 4-ATP-TNT charge-transfer Meisenheimer complex.[33] The UV-vis spectrum in Fig. S6† showed 4-ATP and TNT formed a new absorption peak at 525 nm, which highlights the formation of π–π conjugated structures. We further evaluated the SERS activity of 4-ATP on $Au@SiO_2@Ag@SiO_2$ by immersing into 4-ATP with the concentration from 10^{-16} M to 10^{-10} M. The Raman spectra were shown in Fig. 4. Six characteristic peaks of 4-ATP at 1075, 1143, 1188, 1393, 1438 and 1578 cm^{-1} were clearly identified. In detail, the characteristic peaks of

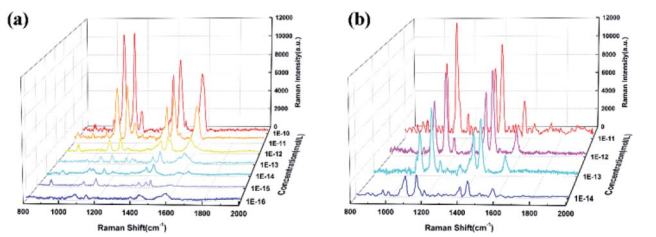

Fig. 4 (a)SERS spectra of 4-ATP in range from 10^{-16} M to 10^{-10} M. (b) SERS spectra of TNT in the range from 10^{-14} M to 10^{-11} M on the 4-ATP-modified $Au@SiO_2@Ag@SiO_2$ nanoparticles.

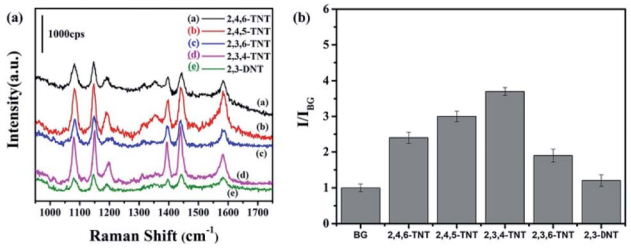

Fig. 5 (a) SERS spectra of 10^{-12} M (a) 2,4,6-TNT (b) 2,4,5-TNT (c) 2,3,6-TNT (d) 2,3,4-TNT (e) 2,3-DNT. (b) Average Raman intensity of 10–12 M TNT and DNT at characteristic absorption band. (I is the Raman intensity of analytes, I_{BG} is the Raman intensity of background).

1578 cm^{-1} due to the C–C ring stretching vibration and 1075 cm^{-1} due to the C–S ring stretching vibration. And the characteristic peaks of 1393 cm^{-1} can be assigned to C–H in-plane vibration. These characteristic peaks are observed typically even at a concentration as low as 10^{-16} M. Thereafter, the next series of experiments were focused on the Raman response of the nitrobenzene compound. Fig. 4b presents the result of SERS signals of 2,4,6-TNT with different concentration on the 4-ATP-modified Au@SiO_2@Ag@SiO_2 nanoparticles. Detection limit of TNT could be down to 2.27×10^{-6} ppb (10^{-14} M).

Universality detection of the nitroaromatic

SERS signals of the nitroaromatic compounds 2,4,6-TNT, 2,4,5-TNT, 2,3,6-TNT, 2,3,4-TNT and 2,3-DNT were shown in Fig. 5a. Raman intensity of DNT and TNT were exhibited in Fig. 5b for clear contrast. It was obvious DNT (e) exhibited a weaker SERS enhancement than TNT. As the DNT molecule structure lacked an electron-withdrawing nitro group, the negative charges could not be dispersed throughout the entire aromatic ring.[34] In this case, DNT cannot form visible absorption at 525 nm in the UV-vis spectrum (Fig. S6†) because it could not construct an interaction complex with 4-ATP. It was also shown that the Raman intensity of 2,3,4-TNT was higher than other TNT molecules because the absorbance of 2,3,4-TNT was the highest at the wavelength of 633 nm as shown in Fig. S6.† In this study, 10^{-12} M for each analyte can be detected, revealing the good sensitivity and universal application of this SERS sensor. Remarkably, Fig. S7† shows the SERS spectrum of 10^{-12} M nitrobenzene on 4-ATP functionalized Au@SiO_2@Ag@SiO_2. It exhibited the Raman fingerprint character of nitrobenzene, which was different from that of TNT and DNT. For example, the peaks at 1012, 1353 cm^{-1} were the characteristic vibrational patterns of NB, which were absent from the SERS spectra of TNT molecules.[35]

Conclusions

In summary, we have prepared a nanostructured hybrid Au@SiO_2@Ag@SiO_2 enhancing the surface plasmon resonance effect and generating an AFE of 5×10^6 which showed the greatly SERS effect. Within the core–triple shells nanostructure, Au@SiO_2@Ag@SiO_2 improved higher signal enhancement than other particles. The results of experiments and 3D-FDTD simulations showed that dual SiO_2 layers can enhance the surface plasmon resonance effect and SERS effect due to the interfacial effects of the long-range plasmon transfer and shell-isolated nanoparticle-enhancement of Au@SiO_2@Ag@SiO_2. To explore the application prospect of the prepared substrate, TNT was selected as the detecting sample. Detection limit of TNT can be down to 2.27×10^{-6} ppb (10^{-14} M) with excellent versatility in detecting nitroaromatic compounds and the particles were universal for nitrobenzene compounds determination. We hope this study will provide illumination for photoelectricity and rapid detection in the future.

Conflicts of interest

There are no conflicts to declare.

Acknowledgements

This work was supported by the National Key Research and Development Program of China (2017YFA0206902, 2017YFA0206900).

References

1 P. K. Jain, X. Huang, I. H. El-Sayed and M. A. El-Sayed, *Acc. Chem. Res.*, 2008, **41**, 1578–1586.
2 P. K. Jain, W. Huang and M. A. El-Sayed, *Nano Lett.*, 2007, **7**, 2080–2088.
3 H. Wang, D. W. Brandl, F. Le, P. Nordlander and N. J. Halas, *Nano Lett.*, 2006, **6**, 827–832.
4 A. J. Haes and R. P. Van Duyne, *J. Am. Chem. Soc.*, 2002, **124**, 10596–10604.
5 A. Marimuthu, J. Zhang and S. Linic, *Science*, 2013, **339**, 1590–1593.
6 X. Cheng, W. Zhang, Y. Ji, J. Meng, H. Guo, J. Liu, X. Wu and H. Xu, *RSC Adv.*, 2013, **3**, 2296–2305.
7 J. Zuo, D. Sun, L. Tu, Y. Wu, Y. Cao, B. Xue, Y. Zhang, Y. Chang, X. Liu and X. Kong, *Angew. Chem., Int. Ed.*, 2018, **57**, 3054–3058.
8 G. Félix, M. Mikolasek, G. Molnár, W. Nicolazzi and A. Bousseksou, *Eur. J. Inorg. Chem.*, 2018, **2018**, 435–442.
9 A. H. Lu, E. e. L. Salabas and F. Schüth, *Angew. Chem., Int. Ed.*, 2007, **46**, 1222–1244.
10 A. Burns, H. Ow and U. Wiesner, *Chem. Soc. Rev.*, 2006, **35**, 1028–1042.
11 J. Shen, Y. Zhu, X. Yang, J. Zong and C. Li, *Langmuir*, 2012, **29**, 690–695.
12 K. Aslan, M. Wu, J. R. Lakowicz and C. D. Geddes, *J. Am. Chem. Soc.*, 2007, **129**, 1524–1525.
13 J. F. Li, Y. F. Huang, Y. Ding, Z. L. Yang, S. B. Li, X. S. Zhou, F. R. Fan, W. Zhang, Z. Y. Zhou and B. Ren, *Nature*, 2010, **464**, 392.
14 T. Hirakawa and P. V. Kamat, *J. Am. Chem. Soc.*, 2005, **127**, 3928–3934.
15 C. Huang, C. Xu, J. Lu, Z. Li and Z. Tian, *Appl. Surf. Sci.*, 2016, **365**, 291–295.

16 A. O. Govorov and I. Carmeli, *Nano Lett.*, 2007, **7**, 620–625.
17 J. Xu, Y.-J. Zhang, H. Yin, H.-L. Zhong, M. Su, Z.-Q. Tian and J.-F. Li, *Adv. Opt. Mater.*, 2018, **6**, 1701069.
18 J.-F. Li, J. R. Anema, T. Wandlowski and Z.-Q. Tian, *Chem. Soc. Rev.*, 2015, **44**, 8399–8409.
19 Y. Wang, J. Zhai, Y. Song, J. Lin, P. Yin and L. Guo, *Adv. Mater. Interfaces*, 2015, **2**, 1500383.
20 J. J. Feng, U. Gernert, P. Hildebrandt and I. M. Weidinger, *Adv. Funct. Mater.*, 2010, **20**, 1954–1961.
21 Z. Yang, J. Aizpurua and H. Xu, *J. Raman Spectrosc.*, 2009, **40**, 1343–1348.
22 T. Ming, L. Zhao, Z. Yang, H. Chen, L. Sun, J. Wang and C. Yan, *Nano Lett.*, 2009, **9**, 3896–3903.
23 X.-W. Chen, V. Sandoghdar and M. Agio, *Nano Lett.*, 2009, **9**, 3756–3761.
24 A. Hakonen, P. O. Andersson, M. S. Schmidt, T. Rindzevicius and M. Käll, *Anal. Chim. Acta*, 2015, **893**, 1–13.
25 D.-K. Lim, I.-J. Kim and J.-M. Nam, *Chem. Commun.*, 2008, 5312–5314.
26 M. W. Forbes and R. A. Jockusch, *J. Am. Soc. Mass Spectrom.*, 2011, **22**, 93–109.
27 W. Xu, N. Mao and J. Zhang, *Small*, 2013, **9**, 1206–1224.
28 C.-C. Chang, K.-H. Yang, Y.-C. Liu, T.-C. Hsu and F.-D. Mai, *ACS Appl. Mater. Interfaces*, 2012, **4**, 4700–4707.
29 R. G. Freeman, M. B. Hommer, K. C. Grabar, M. A. Jackson and M. J. Natan, *J. Phys. Chem.*, 1996, **100**, 718–724.
30 E. Le Ru, E. Blackie, M. Meyer and P. G. Etchegoin, *J. Phys. Chem. C*, 2007, **111**, 13794–13803.
31 I. Zoric, M. Zach, B. Kasemo and C. Langhammer, *ACS Nano*, 2011, **5**, 2535–2546.
32 M. Meier and A. Wokaun, *Opt. Lett.*, 1983, **8**, 581–583.
33 C. Vorbeck, H. Lenke, P. Fischer and H.-J. Knackmuss, *J. Bacteriol.*, 1994, **176**, 932–934.
34 S. Graule, M. Rudolph, N. Vanthuyne, J. Autschbach, C. Roussel, J. Crassous and R. Reau, *J. Am. Chem. Soc.*, 2009, **131**, 3183–3185.
35 X. Liu, L. Zhao, H. Shen, H. Xu and L. Lu, *Talanta*, 2011, **83**, 1023–1029.